Recent Progress in Methanol-to-Olefins (MTO) Catalysts

Miao Yang, Dong Fan, Yingxu Wei, Peng Tian,* and Zhongmin Liu*

Dedicated to Dalian Institute of Chemical Physics, Chinese Academy of Sciences on its 70th anniversary

Methanol conversion to olefins, as an important reaction in C1 chemistry, provides an alternative platform for producing basic chemicals from non-petroleum resources such as natural gas and coal. Methanol-to-olefin (MTO) catalysis is one of the critical constraints for the process development, determining the reactor design, and the profitability of the process. After the construction and commissioning of the world's first MTO plant by Dalian Institute of Chemical Physics, based on high-efficiency catalyst and fluidization technology in 2010, more attention has been attracted for a deep understanding of the reaction mechanism and catalysis principle, which has led to the continuous development of catalysts and processes. Herein, the recent progress in MTO catalyst development is summarized, focusing on the advances in the optimization of SAPO-34 catalysts, together with the development efforts on catalysts with preferential ethylene or propylene selectivity.

1. Introduction

Molecular sieves with regular microporous architectures, large area surface, and strong acidity have been proved to be the most efficient shape-selective catalysts which have been widely used in many heterogeneous catalytic processes.[1] A well-known example is the discovery of methanol to hydrocarbon reaction and methanol-to-olefin (MTO) reaction by researchers of Mobil in 1977 using aluminosilicate zeolite as the catalyst.[2] Since then, zeolite-catalyzed methanol conversion reaction has drawn considerable attention from both the academia and industry, and breakthroughs have been achieved in the reaction mechanism understanding,[3] high-efficiency catalyst design and preparation,[4] process development, and commercialization.[5]

After extensive experimentation of various molecular sieves with different pore networks, small pore 8-membered ring (8-MR) molecular sieves were demonstrated to be more shape-selective toward light olefins. The small pore openings could prevent the diffusion of larger reaction intermediates (such as higher olefins and aromatics) from the channels, and consequently lead to a high selectivity of ethylene and propylene.[3a,6]

Prof. M. Yang, Dr. D. Fan, Prof. Y. Wei, Prof. P. Tian, Prof. Z. Liu
National Engineering Laboratory for Methanol to Olefins
Dalian National Laboratory for Clean Energy
Dalian Institute of Chemical Physics
Chinese Academy of Sciences
Dalian 116023, China
E-mail: tianpeng@dicp.ac.cn; liuzm@dicp.ac.cn

The ORCID identification number(s) for the author(s) of this article can be found under https://doi.org/10.1002/adma.201902181.

Among the 8-MR molecular sieves, silicoaluminophosphate SAPO-34 with 3D channels and moderate acid strength represents the most interesting one, the light olefins selectivity of which could reach up to 90% or even higher.[7] The excellent MTO performance of SAPO-34 was first reported by Dalian Institute of Chemical Physics (DICP) in 1990.[8] The researchers also demonstrated the good regeneration stability and high-temperature steam stability of SAPO-34.[9] Inspired by these pioneering discoveries, extensive research efforts have been devoted to SAPO-34 focusing on the elucidation of its crystallization mechanism, synthesis optimization, and the relevant catalytic studies, which greatly promote the technological development of the MTO process.

Although SAPO-34 exhibits high catalytic activity and high selectivity toward light olefins, it suffers a rapid deactivation due to the coke deposition. Moreover, the MTO reaction on SAPO-34 catalyst is highly exothermic. These features determine that the industrial MTO process based on SAPO-34 catalyst has to adopt fluidized bed reactor, which allows efficient heat transfer and enables the continuous regeneration of the catalyst. In 2010, the world's first commercial MTO unit was successfully commissioned in Baotou, China by DICP (named DMTO technology).[5,10] The production capacity of ethylene and propylene is 0.6 Mt a^{-1}. To supply commercial catalysts for the DMTO unit, a 2000 t a^{-1} catalyst manufacturing plant was started up in Dalian in 2008. Afterward, DICP developed the DMTO-II technology, in which the byproducts of C$_4^+$ are separated and introduced into a fluidized-bed cracking reactor to improve the yields of ethylene and propylene. Both the cracking unit and the MTO unit share one regenerator and use the same catalyst. By the end of 2018, thirteen DMTO units have been put into operation with a total production capacity of 7.16 Mt a^{-1}. Moreover, DICP launched the new generation of DMTO catalyst and completed the pilot test of the DMTO-III technology in 2018, both of which aim to further improve the olefins yield of DMTO units. The catalyst and technology development of the DMTO process are summarized in **Figure 1**.

Based on SAPO-34 catalyst, UOP and Norsk Hydro also developed an MTO process with a low-pressure fast fluidized-bed reactor.[11] In 2013, a commercialized MTO plant (0.3 Mt a^{-1} olefins) was commissioned in Nanjing, China, which combines the UOP/Hydro MTO process and the total/UOP olefin cracking process to enhance the yield of ethylene and propylene. In addition, Shanghai Research Institute of Petrochemical Technology

**ADVANCED
SCIENCE NEWS**

www.advancedsciencenews.com

**ADVANCED
MATERIALS**

www.advmat.de

(SRIPT) claimed the development of the SMTO technology using SAPO-34-based catalyst and fluidized-bed reactor.[12]

Besides SAPO-34, ZSM-5 with 3D intersected 10-MR channels also attracts considerable attention, which indeed serves as an important role in the development of methanol-to-gasoline (MTG) and MTO processes. The Lurgi company developed a fixed-bed methanol-to-propene (MTP) process based on the ZSM-5 catalyst.[13] The process includes a methanol conversion unit and an ethylene and C_4^+ recycling unit to maximize the propylene yield. In 2011, the first MTP plant using the Lurgi technology (0.5 Mt a^{-1} propylene) was put into operation in Ningxia, China.

The large-scale industrialization of the MTO process achieved in the past decade greatly encourages the research and development of high-performance MTO catalysts in order to enhance the process efficiency. The successful development of a commercial MTO catalyst involves many scientific and engineering challenges: 1) catalyst design with desirable properties, in which, besides olefin yield, long-term catalyst stability, minute side products, operation window, etc., are also important considerations; 2) cost competitiveness of the catalyst; 3) the feasibility and reproducibility of scale-up including molecular sieve synthesis and catalyst preparation; 4) environmental requirements, for which high production efficiency and low waste emissions are highly preferred.

2. Fundamental Understanding on the Zeolite-Catalyzed MTO Reaction

Aiming at realizing the rational design of highly efficient MTO catalysts, researchers have devoted great efforts toward understanding the reaction mechanism at the molecular and chemical bond level. According to the previous investigations and the very recent progress on the formation of the first C—C bond,[3,14] it is believed that zeolite-catalyzed MTO reaction follows an inefficient direct mechanism in the initial reaction period and then an indirect pathway (dual-cycle mechanism) in the subsequent high activity period. Based on the spectroscopic evidences and theoretical calculations, several direct mechanisms have been proposed, including carbonylation-based mechanism,[15] methoxymethyl cation mechanism,[16] methane-formaldehyde mechanism,[17] carbene insertion mechanism,[18] and methoxy-mediated DME/methanol activation mechanism.[14] Clearly, more works are needed to reach a fully understanding of the initial C—C bond generation. On the contrary, the indirect dual-cycle mechanism is better understood, which involves the aromatic-based hydrocarbon pool (HCP) mechanism and the olefins methylation/cracking mechanism.[19] In the aromatic-based cycle, methylbenzenes and their protonated counterparts work as the active intermediates, to which the methanol feed is attached and from which the olefin products are eliminated. It has been recognized that methylbenzenes with two or three methyl groups predominantly deliver ethylene, while higher methylbenzenes favor the generation of propylene and butylene;[3a,20] the types of formed HCPs are strongly dependent on zeolite topology, acidity, and reaction condition. In the olefin-based route, higher olefins formed by the methylation of light olefins act as reactive species, which

Yingxu Wei received her Ph.D. at Dalian Institute of Chemical Physics (DICP), Chinese Academy of Sciences (CAS) in 2001. She conducted her postdoctoral study at the University of Namur (Belgium) from 2003 to 2004. She has been the group leader of Catalysis and New Catalytic Reactions in the National Engineering Laboratory for Methanol to Olefins since 2009 and was promoted to professor in 2011. She has been involved in research on heterogeneous catalysis and methanol to olefin conversion.

Peng Tian received her Ph.D. from Dalian Institute of Chemical Physics, Chinese Academy of Sciences in 2004. She has been the group leader of Molecular Sieves Synthesis in the National Engineering Laboratory for Methanol to Olefins since 2009 and was promoted to professor in 2013. Her research interests are mainly focused on the synthesis and catalysis application of molecular sieves, and methanol conversion reaction.

Zhongmin Liu has been the Director of Dalian Institute of Chemical Physics, Chinese Academy of Sciences since 2017. As a leading scientist, he accomplished the industrial demonstration test of DMTO technology in 2006, based on which the world's first commercial MTO unit was built up. He was elected academician of the Chinese Academy of Engineering in 2015.

mainly crack to propylene and butylene. Ethylene is however only a minor cracking product from higher olefins. **Figure 2** illustrates the proposed reaction network of MTO process,[3c] which includes the initial C—C bond generation, HCP species formation from the initial olefin products, the highly efficient reaction stage via the indirect route, and the deactivation stage resulting from the formation of heavier aromatic coke species.

Both the topologies and acidity of molecular sieves are important factors for the MTO reaction. The channel and cavity structure of molecular sieves can impose spatial confinement effect on the shape/size/reactivity of active intermediates, and affect their

1902181 (2 of 15)
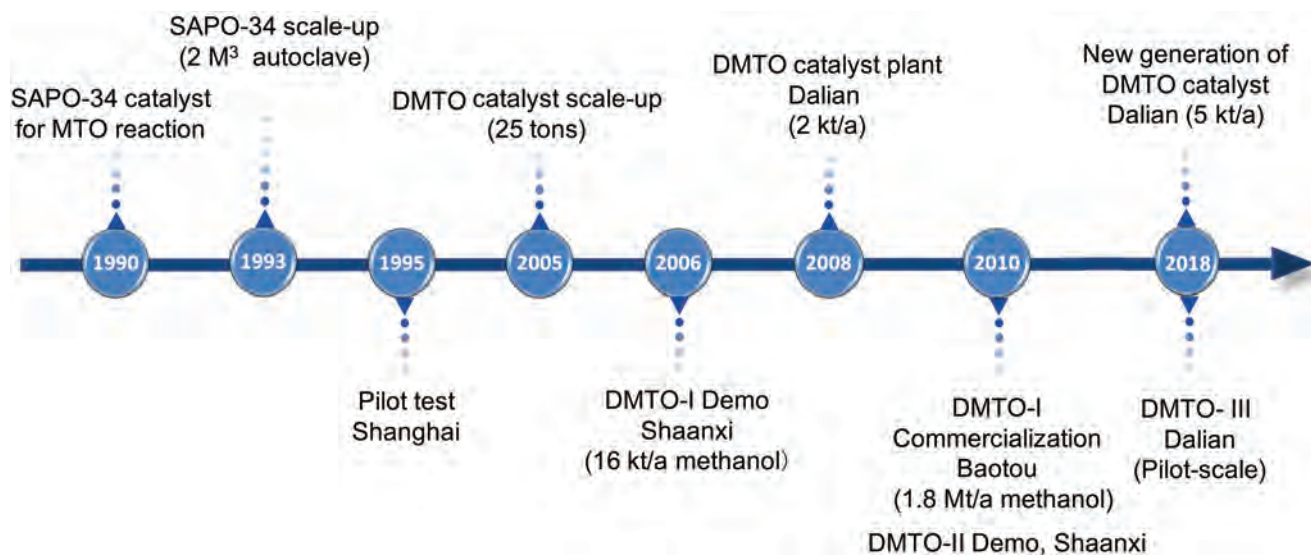
**Figure 1.** Catalyst and technology development of the DMTO process.

reaction routes and product selectivity. The Brønsted acid sites are the essential driving force for the occurrence of MTO reaction. The generation and evolution of the active intermediates are closely related to the acid properties of molecular sieve catalysts. Therefore, the choice of topology and the tuning of acidity are crucial for the improvement of the catalyst performance.

Molecular sieves with 8-MR openings and cavity structures have received considerable attention due to their high selectivity to light olefins in the MTO reaction. The narrow 8-MR pore openings could impose diffusion limitations on large molecules and make light olefins the dominant products (product-shape selectivity). Besides the pore openings, the cavity structures also play important roles in the reaction. The shape of the cavities governs the configuration and reactivity of the active intermediates via a host–guest confinement effect. Liu and co-workers systematically investigated the methanol conversion on SAPO-35 (LEV), SAPO-34 (CHA), SAPO-18 (AEI), and DNL-6 (RHO) with distinct cavity dimensions.[21] Under similar reaction conditions, different product spectra on the catalysts were observed. SAPO-35 with the smallest cavities (0.73×0.63 nm) exhibited higher selectivity toward ethylene; SAPO-34 (1.09×0.67 nm) yielded ethylene and propylene as the main products; SAPO-18 and DNL-6 with larger cavity space (1.27×1.16 nm

for the former and 1.14×1.14 nm for the latter) delivered propylene and butylene in high selectivity. With the aid of $^{12}C/^{13}C-CH_3OH$ switch experiments and theoretical calculations, it was concluded that the sizes of the confined active species were controlled by the cavity sizes (**Figure 3**). This finding can be further correlated with the product selectivity, that is, in smaller cavities, lower methylbenzenes predominantly form and present high reactivity as the active intermediates, which favor the production of ethylene; in larger cavities, higher methylbenzenes appear as the active species, which preferentially lead to propylene and butylene. In addition, the catalyst activity could also be linked to the reaction intermediates. As hexamethylbenzene and heptamethylbenzenium cations are the most active HCP intermediates, the reactions involving them are easy to proceed with lower barriers, which explains the high MTO activity on SAPO-34 and DNL-6.[21c] In the contrast, the steric confinement imposed by the small cage of SAPO-35 restrains the generation of bulkier active species with high reactivity, and causes a lower methanol conversion. Besides, it is noted that the 8-MR pore openings might vary with the topologies, affecting the product selectivity and deactivation rate. For example, SAPO-42 with LTA cage (1.14×1.14 nm) and large 8-MR pore sizes (0.41×0.41 nm) was reported to show
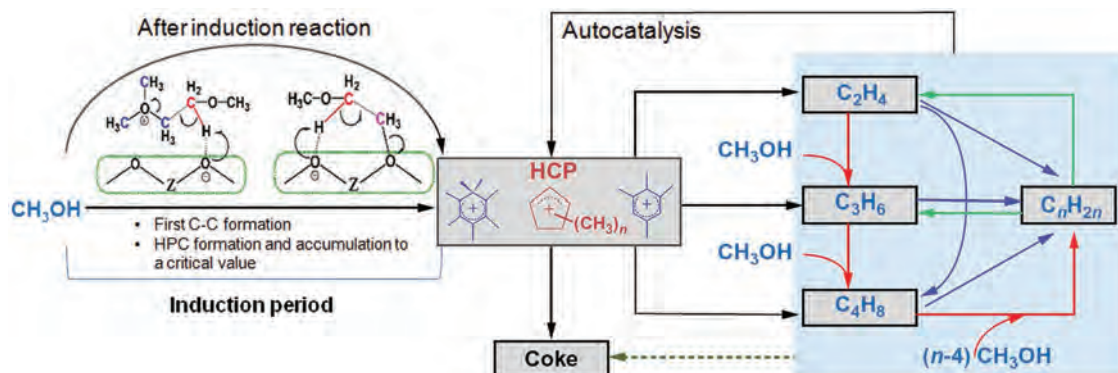
Figure 2. Proposed reaction network of the MTO process. Reproduced with permission.[3c] Copyright 2017, Elsevier.
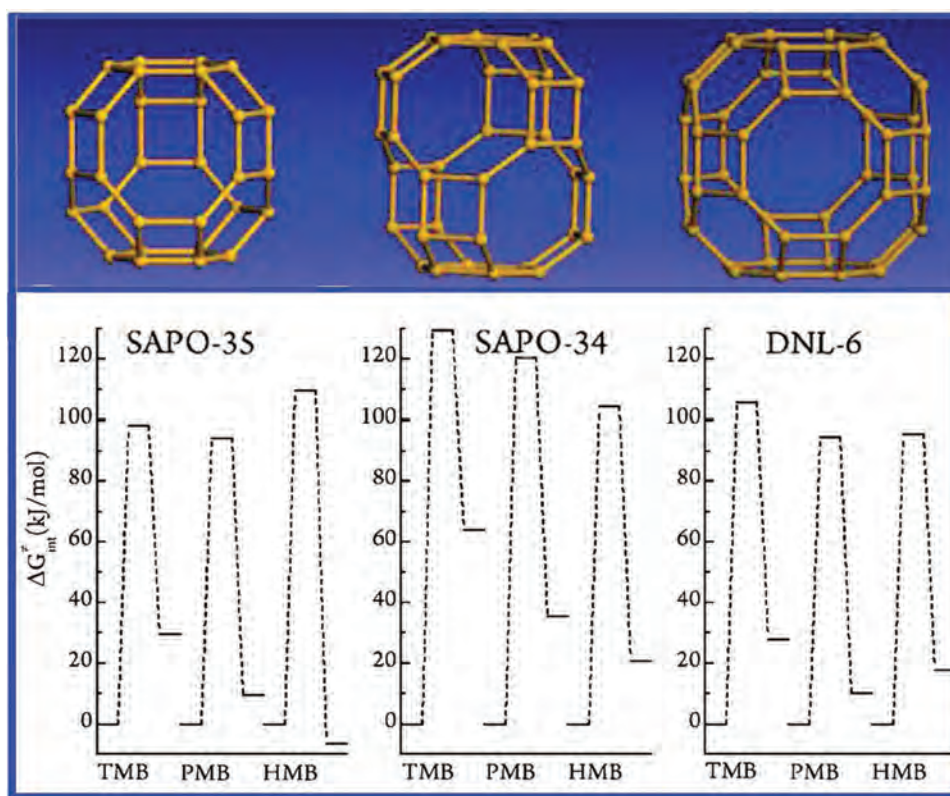
Figure 3. Cavity structures of 8-MR molecular sieves (top) and intrinsic free-energy barriers (275 °C) of the methylation of tetraMB, pentaMB, and hexaMB over SAPO-35, SAPO-34, and DNL-6 (bottom). The estimated barriers drop with the number of methyl groups on SAPO-34 and DNL-6. However, on SAPO-35, the methylation of hexaMB holds the highest barriers. MB refers to methylbenzene. Reproduced with permission.[21c] Copyright 2015, American Chemical Society.

enhanced C_4^+ selectivity, whereas the application of SAPO-56 with large AFX cage (1.30×0.83 nm) and narrow pore sizes (0.34×0.36 nm) gave rise to higher selectivity toward ethylene plus propylene and faster formation of heavy polyaromatic hydrocarbons.[22] These results imply that both the cavity structures and the 8-MR pore openings affect the methanol conversion and product generation. To optimize the ethylene plus propylene yield and achieve longer catalyst lifetime, molecular sieves with medium-sized 8-MR pore opening and cavity dimension seems to be a reasonable choice.

Medium-pore 10-MR molecular sieves represented by ZSM-5 (MFI) are also effective catalysts for the olefins production in methanol conversion reaction. For the catalysts with channel intersections, aromatic- and olefin-based mechanisms can work simultaneously. The shape/size of the aromatic species and their reactivity depend on the dimensions of the intersection cavities, which is similar to the findings for the cavity-type 8-MR molecular sieves. By decreasing the acid density of the catalyst, the olefinic cycle can be effectively promoted, leading to enhanced propylene selectivity and propylene/ethylene ratio, together with notably reduced aromatics selectivity. For ZSM-5 with optimized acidity, a propylene selectivity of 40–50% with a propylene/ethylene ratio of 5–10 can be achieved.[23] ZSM-22 (TON) with 1D channels is another typical representative among the 10-MR molecular sieves. The lack of internal cavity suppresses the aromatic-based cycle and makes olefin-based cycle the prevailing route. C_3–C_5 hydrocarbons dominate the product spectrum with low selectivity of ethylene and aromatics. However, the 1D channel of ZSM-22 tends to cause diffusion limitation, resulting in fast catalyst deactivation.[24] Large-pore 12-MR molecular sieves are generally employed for mechanism elucidation, and Beta zeolite with low Si/Al ratio is the favorite model material.[25] Due to the lack of space limitation and high acid concentration, the aromatics cycle prevails in the reaction, yielding C_4^+ aliphatics and aromatics as the main products.[26] Recently, high-silica Beta zeolites (Si/Al > 100) with low acid density were employed in MTO reaction and yielded a surprising propylene selectivity (up to 58% at 550 °C) together with a high propylene/ethylene ratio (>10) and long lifetime.[27] Mechanism investigation evidenced that the low acid density on the catalyst made olefinic cycle the dominant route, which explains well the observed product distribution. However, the total selectivity of ethylene plus propylene over both 10-MR and 12-MR catalysts is generally lower than 65% due to their relatively large pore openings, which is remarkably inferior to that on 8-MR catalysts.

With respect to the influence of the acidity on the MTO reaction, it has been recognized that excess Brønsted acid sites can enhance the possibility of successive reactions when the generated hydrocarbons escape from the channels to the effluent; higher acid strength could increase the secondary reaction rates and aggravate the retention of coke precursors.[28] Both circumstances could accelerate the coke formation and cause a shortened catalyst lifetime and a reduced olefin selectivity.

ADVANCED
SCIENCE NEWS

www.advancedsciencenews.com

ADVANCED
MATERIALS

www.advmat.de

Hence, the catalysts with mild acid strength and relatively low acid density (e.g., low-silica SAPOs) should be more appropriate for the MTO reaction, which can slow down the coke deposition and achieve longer catalytic lifetime. Moreover, the alleviated side reactions could facilitate the improvement of olefin selectivity.[28c] In principle, lower acid density or weaker acid strength increases the contribution of the olefinic cycle. Chen et al. investigated the MTO reaction activity and mechanism on small pore AlPO-18 and low-silica SAPO-18s (Si/(Si+Al+P) = 0.014, 0.052).[29] The methanol conversion and the formation/accumulation of active HCP species were found to rise with the increase of Brønsted acid density of the catalysts. Over nonacidic AlPO-18 catalyst, the methanol conversion was very low and the reaction mainly followed the olefinic route; for SAPO-18 with lower Brønsted acid density of 0.246 mmol g^{-1}, two cycles were involved for the formation of olefins; for SAPO-18 with relatively high acid density (0.568 mmol g^{-1}), the aromatics mechanism became the dominant route. Moreover, investigations on the MTO reaction over low-silica SAPO-34s showed that long catalyst lifetime and high selectivity toward ethylene plus propylene could be concomitantly achieved on SAPO-34 with a Brønsted acid density of 0.52 mmol g^{-1};[30] further lowering the acid density of SAPO-34 (0.39 mmol g^{-1}) led to a shortened lifetime, likely resulted from the insufficient acid sites. It implies that for one specific molecular sieve, acid density is a critical parameter for selectivity optimization and lifetime extension. The acid density should be tuned at relatively low, but appropriate level to achieve long catalyst lifetime and optimized light olefins selectivity.

Apart from the topology and acidity, crystal size is another important factor affecting the MTO performance of the molecular sieve catalysts. Decreasing the crystal size or introducing mesopores into the crystals has been demonstrated to be effective strategies to reduce the diffusion limitation and side reactions, which could slow down the coke deposition and prolong the catalyst lifetime.[31] For 8-MR molecular sieves such as SAPO-34, decreasing the crystal size was found to have little impact on the selectivity of the catalysts at comparable coke content.[32] However, for 10-MR and 12-MR materials, small crystal sizes or hierarchical structures may give rise to an increased selectivity to heavier products along with the prolonged lifetime.[26,33] It is noted that internal defects may be created in the aluminosilicate crystals while synthesizing nanocrystallines or introducing mesopores,[34] which would partially offset the positive effect of shortened diffusion path. However, the influence of lattice defects in SAPO crystals on methanol conversion is yet to be identified.

3. Synthesis and Optimization of SAPO-34 Catalyst

The formation of SAPO framework could be considered as the incorporation of Si atoms into the neutral AlPO$_4$ framework, generating bridged Si(OH)Al hydroxyls (Brønsted acid sites) with milder acidity than its aluminosilicate analogue. The chemical environment of Si atoms generally becomes complex from single Si(4Al) species to its coexistence with Si islands as the increase of Si content. The Si(nAl) species (n = 1, 2, 3), located at the margin of the Si islands, have been acknowledged

to possess relatively strong acidity compared to Si(4Al) species.[35] Up to now, SAPO-34 is still the most effective MTO catalyst owing to its small 8-MR window, unique CHA cavity structure, medium/strong acidity, and excellent hydrothermal stability. Considerable efforts have been invested to improve the ethylene plus propylene selectivity and alleviate the deactivation of SAPO-34 catalysts. The optimization strategies include the tuning of the acidity, mainly by Si manipulation in the SAPO-34 framework, and the preparation of crystals with small sizes or hierarchical porosities. Relatively low acid density (low Si content) with mild acid strength generated from Si(4Al) species is highly desirable for the MTO reaction, as summarized in Section 2. In this section, the advances in Si environments control, synthetic strategies of low-silica SAPO-34 and nanosized/mesoporous SAPO-34, as well as their catalytic performance are reviewed.

3.1. Organic Template and Si Chemical Environment

Organic template is indispensable for the crystallization of SAPO materials. The choice of organic template could influence the capacity of Si incorporation and the local Si environments. Over 30 templates have been reported to be able to direct the structure of SAPO-34. Tetraethylammonium hydroxide (TEAOH) is one of the most powerful templates which can direct the crystallization of SAPO-34 with relatively low Si content.[36] Only one TEAOH molecule can be accommodated in each CHA cage, due to its relatively large molecular dimension. Theoretically, the upper limit of Si content (termed as Si/(Si+Al+P)) for the existence of single Si(4Al) environment is 0.083 in TEAOH-templated SAPO-34, which corresponds to one Si atom per CHA cage (12 T atoms) balanced by one template cation. With the further increase of the Si content, the formation of Si islands becomes inevitable in order to keep the charge balance between the negative SAPO framework and template cations. It is noted that the crystallization of Si-enriched SAPO-34 by TEAOH template is difficult. Meanwhile, the Si content of SAPO-34 templated by TEAOH cannot be reduced indefinitely because SAPO-18/34 intergrowth phase or even pure SAPO-18 may form at a low silica dosage.[37] Triethylamine (TEA) is another large and common template for the synthesis of SAPO-34. It indeed directs a phase of SAPO-34/18 intergrowth with CHA as the majority although relatively low Si content (≈0.06) can be achieved.[38] The ethylene plus propylene selectivity in MTO reaction on such kind of material is lower than that on SAPO-34 with pure CHA structure.[39] This is reasonable as discussed in Section 2. The larger AEI cages of SAPO-18 favor the formation of larger active intermediates, which prompt the formation of propylene and butylene. Therefore, it is important to avoid the AEI intergrowth while synthesizing the SAPO-34 catalyst. Morpholine (MOR) and diethylamine (DEA) are two small templates which can be doubly accommodated in one CHA cage. This also explains the higher Si incorporation and more Si(4Al) species in the DEA- and MOR-directed products. The Si content of SAPO-34–DEA and SAPO-34–MOR is generally higher than 0.09.[40]

To expand the templates for SAPO-34 synthesis is attractive for both industry and academia, which can offer more

ADVANCED
SCIENCE NEWS
www.advancedsciencenews.com

ADVANCED
MATERIALS
www.advmat.de
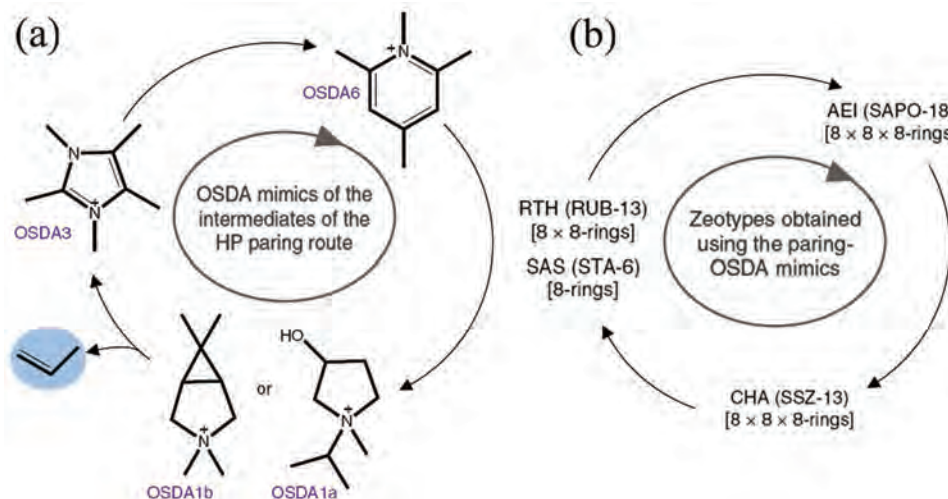
Figure 4. a) Proposed organic structure-directing agent mimics of the different intermediates present in the HCP paring route. b) Zeotypes obtained using these mimics. Reproduced with permission.[47] Copyright 2018, Springer Nature.

opportunities for the optimization of SAPO-34 catalyst. Fan et al. developed an aminothermal process to synthesize SAPO-34 where organic amine was used as both the dispersing medium and the template.[41] In such a system, a variety of organic amines including diisopropylamine (DIPA), N,N,N',N'-tetramethylethylenediamine (TMEDA), diglycolamine, and diisopropanolamine have been found to be capable of directing SAPO-34 with high solid yield.[42] Subsequently, DIPA was found to function well in the hydrothermal synthesis of SAPO-34.[43] Compared with the isomeric dipropylamine (DPA) template, an enhanced crystallization rate and solid yield were observed for the DIPA-templated synthesis, owing to the higher efficacy of DIPA template as rationalized by theoretical simulation. The lower Si content (lower acid density), weaker acid strength (single Si(4Al) environment), and relatively uniform Si distribution in the crystals corporately helped SAPO-34–DIPA exhibit longer lifetime and higher olefin selectivity. Very recently, Yan et al. determined the locations and orientations of four templates cyclohexylamine (CA), n-butylamine (BA), DIPA, and DPA in the CHA cage of SAPO-34/44 through Rietveld refinement and simulated annealing against PXRD data.[44] It was found that one CHA cage could be occupied by either two templates (CA and BA) in the up-and-down arrangement or one template (DIPA and DPA) in the longitudinal configuration. Different cell parameters observed for these SAPO-34s suggest their distinct microstructures, which may also contribute to the deviation of light olefin selectivity on these samples. Based on the understanding of the configuration of template molecules in the SAPO crystals, we developed a novel approach called RSS (refining, summarizing, and searching) to identify appropriate templates for synthesizing specific SAPO materials.[45] Adopting the RSS approach, the template reserve of a small pore SAPO material DNL-6 has been extended from two types to fourteen additional commercial ones. Besides, Corma and co-workers proposed a new template-design strategy by mimicking the transition states of some pre-established chemical reactions.[46] They synthesized cavity-type small pore SSZ-13, SAPO-18, and RUB-13 using the mimics of the hydrocarbon

pool intermediates (shown in **Figure 4**) as organic template. The materials obtained were capable of performing the MTO reaction.[47] Hopefully, these efforts and findings might help find more powerful templates to prepare SAPO materials with excellent MTO catalytic performance.

3.2. Synthesis of Low-Silica SAPO-34

Fluoride-mediated route has been demonstrated to be effective for low-silica SAPO-34 synthesis, because fluoride can stabilize the AlPO$_4$-34 framework by the coordination formation of Al–(μ$_2$-F)$_2$–Al units.[48] With the assistance of fluoride, Dai et al. synthesized a series of SAPO-34 with varied Si content (0–0.05) using MOR template and investigated their MTO performances.[49] The sample with a Si content of 0.03 (Brønsted acid density: 0.32 mmol g^{-1}) exhibited the longest catalytic lifetime due to the well-balanced olefinic and aromatics cycles. SAPO-34 with extremely low Si content deactivated faster due to the coverage of acid sites instead of channel blockage. Besides the stabilizing effect for the framework of low-silica SAPO-34, F$^-$ ions could also help optimize the Si coordination environment. Xu et al. investigated the effect of HF in the synthesis of SAPO-34 using TEA as the template, and found that the proportion of Si(4Al) species rose gradually with the increase of F$^-$ ion content in the initial gel.[50]

Since the introduction of fluoride is not welcome in industries due to the corrosion problems, endeavors toward the fluoride-free synthesis of low-Si SAPO-34 are also carried out. Hitherto, to prepare SAPO-34 with adjustable Si content lower than 0.06 without fluoride media still remains challenge. To decrease Si dosage in the initial gel or shorten crystallization time is certainly an easy approach to reduce the Si content in the products. However, the resultant materials often contain impurities when employing a low Si dosage. Also, insufficient crystallization time may give rise to low crystallinity and solid yield. Recently, Gao et al. found that the efficiency of Si incorporation dropped at low temperature, resulting in a decreased Si content in the

**ADVANCED
SCIENCE NEWS**

www.advancedsciencenews.com

**ADVANCED
MATERIALS**

www.advmat.de

SAPO-5 product.[51] In addition, the crystal growth habit was also changed and led to the fabrication of SAPO-5 nanosheet assemblies with different morphologies. With this experience, Gao et al. further employed the low-temperature synthesis approach to prepare SAPO-34 and succeeded in the preparation of low-silica SAPO-34.[30] The lowest Si content, achieved at a crystallization temperature of 120 °C, was around 0.039. The best MTO catalytic performance (both selectivity and lifetime) was found to be reached on SAPO-34 with a Si content of 0.047 (Brønsted acid density: 0.52 mmol g^{-1}). When using SAPO-34 with the lowest Si content of 0.039 as the catalyst, a shortened lifetime was observed, despite the high olefin selectivity.

### 3.3. Synthesis of Mesoporous/Nanosized SAPO-34

3.3.1. Soft-Template-Assisted Method

Synthesis of mesoporous SAPO-34 by hard templates is relatively scarce. The main problem hindering its application lies in the weak interactions between the hard template and the inorganic gel. In contrast, soft templates like surfactants are well-acknowledged to be more flexible and efficient for the morphology control due to their designability and self-assembly properties. The strong interactions between the soft template and the inorganic source could effectively help avoid the phase separation between microporous and mesoporous structures.

Organosilane surfactants with long alkyl chain and quaternary ammonium groups like [3-(trimethoxysilyl)propyl]octadecyldimethylammonium chloride (TPOAC) are widely employed soft templates for the preparation of mesoporous SAPO-34. The morphology of SAPO-34 was found to be related with both the choice of microporous templates and the dosage of the mesoporogen. **Figure 5** shows the images of SAPO-34s synthesized using four different microporous templates together with TPOAC.[52] Cubic agglomerates of small nanocrystals were formed when MOR was used as the template.[52a] The morphology became spherical nanosheet assembly when DEA was used under the similar crystallization conditions.[52b] In TEA-templated system, the crystals further evolve into cubic assemblies of nanosheets.[52c] A common feature is that all the crystals are in the form of nanoassemblies with large secondary particle size, in contrast to the traditional rhombohedral single crystals of SAPO-34,

obviously due to the self-assembly function of the introduced surfactants. Notably, the creation of Si defect sites (Si—OH) is inevitable with the removal of the introduced organosilanes, which in turn leads to a mismatch between the acidities and the Si content of SAPO-34. Compared with traditional SAPO-34 of similar Si content, SAPO-34 prepared in the presence of organosilanes is expected to be inferior in both the acid strength and density. Although the preparation of mesoporous SAPO-34 was successfully achieved when mesoporogen was introduced, an obviously retarded crystallization process and a narrow crystallization phase region could be observed in such systems. A large amount of ball-milled SAPO-34 precursor was subsequently introduced, and the crystallization of mesoporous SAPO-34 can be completed within 4 h. This method is nominated as a reconstruction strategy.[53] As shown in the left column of **Figure 6**, the SAPO-34 product exhibits uniform 300–500 nm dice-like particles with rough surface. Each particle is composed of 20–50 nm nanocrystals with abundant additional auxiliary porosities. The existence of mesopores and their good connectivity with the microporous channels were confirmed by N$_2$ adsorption and variable-temperature laser-hyperpolarized (HP) ^{129}Xe NMR and 2D-NMR exchange spectroscopy (EXSY). The single crystal nature of the particle was confirmed by selected large area electron diffraction (Figure 6, left column). The formation of mesoporous SAPO-34 single crystal could be rationalized by comparing the crystallization curves of the different synthetic systems, as displayed in Figure 6. When TPOAC was added alone, both the nucleation and crystal growth rate were slowed down comparing with the conventional system; the nucleation period was skipped and polycrystal assemblies were achieved with the mere presence of ball-milled SAPO-34 precursor; when TPOAC and the ball-milled precursor coexisted in the gel, the formation rates of microporous and mesoporous structures were well-matched, and thus mesoporous SAPO-34 single crystals preferentially formed. The material showed a much better hydrothermal stability than normal mesoporous SAPO-34 thanks to its single crystal feature, which should be attractive for the industrial application.

Various nonsurfactant organosilanes are also explored to replace the expensive TPOAC. 3-piperazinepropylmethyldimethoxysilane (PZPMS), commonly used as a commercial textile finishing agent, is one of the candidates. Wu et al. synthesized SAPO-34 nanocrystal assemblies by using such an additive together with TEA as a microporous template.[39] The
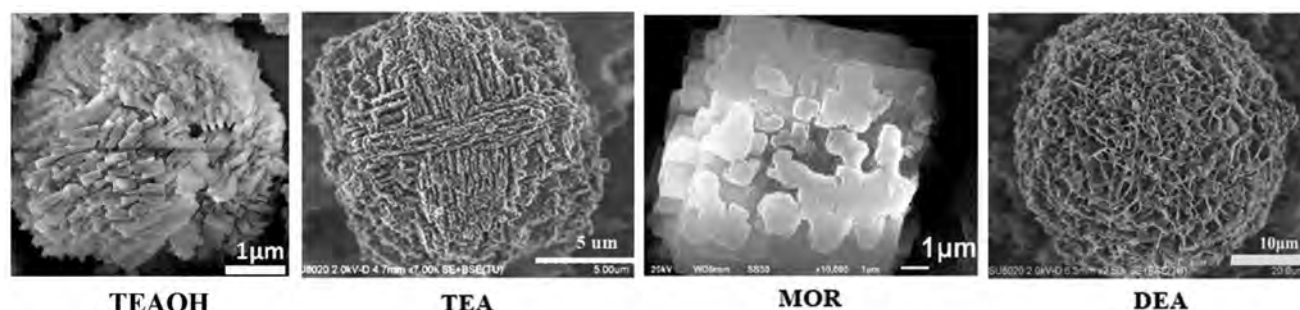
Figure 5. Four different morphologies of SAPO-34s synthesized by mesoporogen TPOAC with different microporous templates. TEAOH image: Adapted with permission.[52d] Copyright 2019, Springer Nature. TEA image: Reproduced with permission.[52c] Copyright 2016, The Author. MOR image: Adapted with permission.[52a] Copyright 2014, Royal Society of Chemistry. DEA image: Adapted with permission.[52b] Copyright 2015, Royal Society of Chemistry.

ADVANCED
SCIENCE NEWS
www.advancedsciencenews.com

ADVANCED
MATERIALS
www.advmat.de
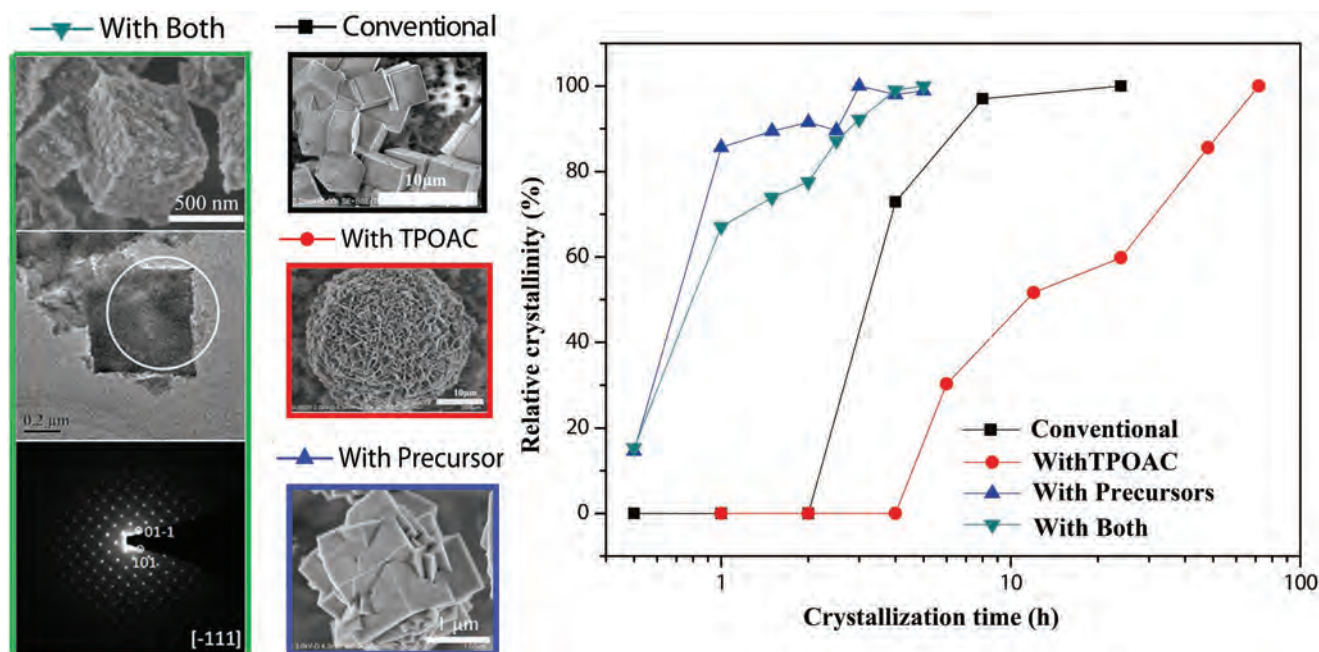
Figure 6. Scanning electron microscopy (SEM) and TEM images of mesoporous SAPO-34 single crystals (left), SAED pattern taken with the selected circle region along the [−111] zone axes (left), SEM images of reference samples (middle), and crystallization curves of SAPO-34 in four different crystallization systems (right). Adapted with permission.[53] Copyright 2016, Royal Society of Chemistry.

PZPMS plays triple functions in the synthesis, i.e., cotemplate, crystal growth inhibitor, and part of the silica source. Importantly, piperazinyl group as a cotemplate can effectively inhibit the intergrowth of SAPO-18/34 phase. The catalytic lifetime was remarkably prolonged together with an enhanced selectivity of light olefins owing to the decreased crystal size and perfect CHA structure. Yang et al. synthesized SAPO-34 nanoaggregates using phenylaminopropyl-trimethoxysilane (PHAPTMS) as part of Si source and TEAOH as a microporous template.[54] The PHAPTMS was grafted on the crystal surface of SAPO-34 with the formation of Si−O−Si−C bonds, which inhibited the crystal growth and modified the acid distribution significantly. Zheng et al. found that phenyltrimethoxysilane (PTMS) could significantly slow down the crystallization rate of SAPO-34 in a TEAOH-templated system.[55] During the hydrothermal crystallization process, the C−Si bond in PTMS cleaved and it was the resultant $Si(OH)_x$ that actually participated in the crystallization. Agglomerated SAPO-34 nanocrystals (≈100 nm) were obtained, which exhibited enhanced catalytic stability in MTO reaction.

To circumvent the impact of Si from organosilanes on the framework acidity, nonsilane organics are extensively explored for SAPO-34 synthesis. Wang et al. designed and employed an organophosphorous surfactant [2-(diethoxylphosphono) propyl] hexadecyldimethylammonium bromide (DPHAB) for mesoporous SAPO-34 synthesis, in combination with various microporous templates.[56] TEAOH showed the best cooperating ability with DPHAB to direct the formation of nanosized and mesoporous SAPO-34. Wu et al. synthesized nanosized SAPO-34 under the assistance of seeds and the presence of bifunctional 1-[2-(2-hydroxyethoxy)ethyl]piperazine (HEEP) or 1-(2-hydroxyethyl)-piperazine (HEP) (**Figure 7**).[57] The resultant samples exhibited improved transport properties and enhanced

MTO catalytic performances. Solid state ^{13}C MAS NMR indicated that the organics decomposed during the crystallization process. Thanks to the accelerated nucleation by seeds, HEEP/HEP took effect before its decomposition. Otherwise, large crystal sizes would be obtained as displayed in Figure 7. A possible crystallization process had been proposed and illustrated in Figure 7g. The piperazinyl groups acted as a cotemplate prompting the formation of pure CHA phase, while the hydroxyl/ether groups helped restrain the crystal growth. Recently, Guo et al. employed a low-cost cationic nonsurfactant polydiallyldimethylammonium chloride (PDADMAC) together with MOR template to synthesize SAPO-34.[58] The PDADMAC molecules were evidenced to be embedded within the SAPO-34 crystals. The existence of abundant intracrystalline mesopores was confirmed by transmission electron microscopy (TEM) images. The prepared SAPO-34 exhibited a remarkably prolonged catalytic lifetime and excellent light olefins selectivity in MTO reaction. Another interesting additive is rapeseed pollen extract.[59] During the hydrothermal treatment, the components of the extract could react with TEA to form new amino-containing compounds, which directed the assembly of SAPO-34 nanosheets into a blossoming flower-like morphology.

3.3.2. Influence of Starting Reactants

Discussions about the effects of Si and Al sources on SAPO-34 crystallization are relatively rare, in spite of their vital roles in synthesis. It has been demonstrated that the Si atoms directly take part in the nucleation of SAPO-34, and the insufficient Si dosage may lead to competitive phases like AFI, AEI, or AEL. In addition, the choice of Si sources may play a crucial role in the shape and size control of SAPO-34 crystals, attributed to

ADVANCED
SCIENCE NEWS
www.advancedsciencenews.com

ADVANCED
MATERIALS
www.advmat.de
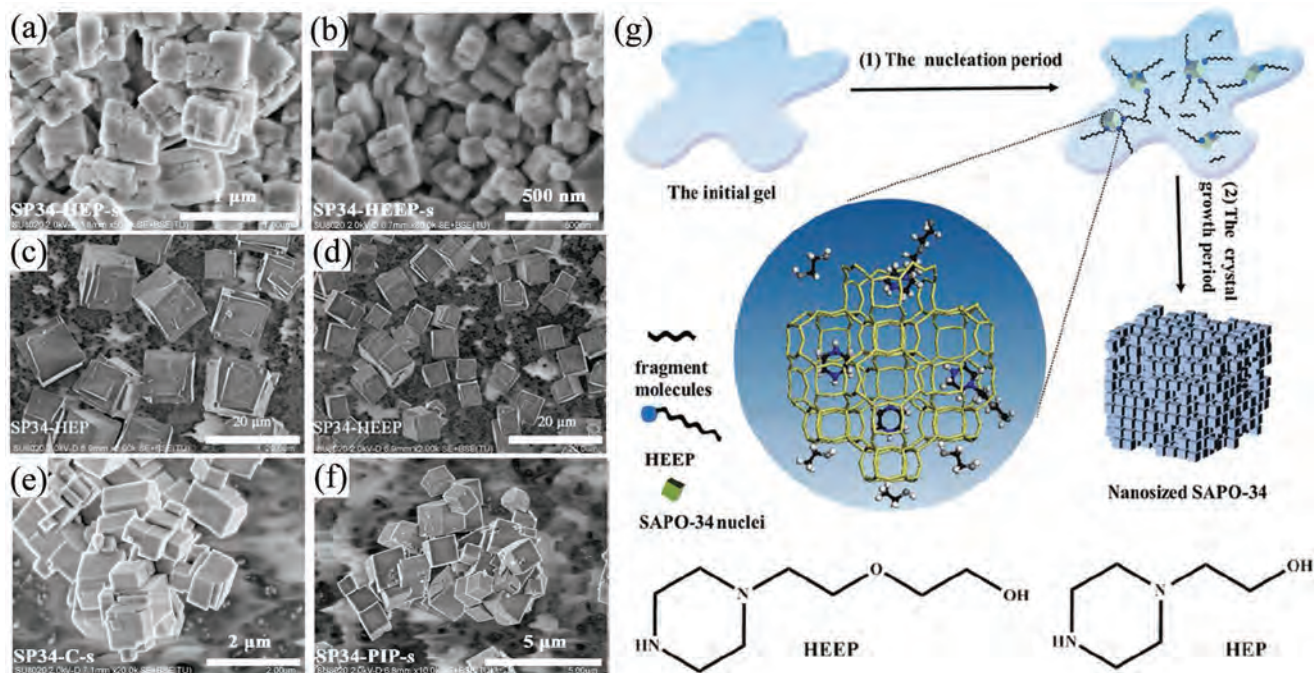
Figure 7. a–f) SEM images of the synthesized SAPO-34 using TEA template: with HEP and seeds (a); with HEEP and seeds (b); with HEP alone (c); with HEEP alone (d); with none (e); and with piperzine (f). g) Proposed formation scheme of nanosized SP34-HEEP-s. TEA molecules in the structures are omitted for clarity. a–g) Adapted with permission.[57] Copyright 2018, Royal Society of Chemistry.

their different solubilities and reactivities. Lin et al. prepared a variety of SAPO-34 crystals using TEAOH as the template.[60] Modified morphologies from nanosheets (≈250 × 50 nm) to uniform nanoparticles (≈100 nm) can be achieved by varying the Si source from colloidal silica to TEOS. Zhu et al. found that mesoporous SAPO-34 could be prepared from a natural layered kaolin material, functioning as both the Si and Al sources, the layered structure of which influenced the crystal growth and the consequent morphology.[61] In contrast, using preshaped kaolin microspheres (30–100 μm) instead would lead to the crystallization of conventional SAPO-34 crystals on the microsphere surface and in the solution. Based on our exploration on the synthesis of mesoporous SAPO-34s, organic Si (ethyl orthosilicate) and Al sources (aluminum isopropoxide) seem to have better interaction with mesoporogen or other organic additives, leading to a facile preparation of mesoporous zeolite product.

Dry gel conversion is another interesting synthetic method featured by the concentrated reactants gel. Such system may offer high concentration of nuclei and slow growth rate, favorable for the preparation of small crystals. Hirota et al. synthesized SAPO-34 nanocrystals by a dry gel conversion method using TEAOH template.[62] The average crystal size was 75 nm. Rimaz et al. synthesized mesoporous SAPO-34 with dry gel conversion method in the presence of carbon nanotubes as a hard template and DEA as a microporous template.[63] Gong et al. synthesized hollow SAPO-34 cubes with a hierarchical structure by the dry gel method.[64] The addition of gelatin in the synthesis was found to be responsible for the formation of the hierarchically organized internal structure. Although the dry gel conversion could be operated easily in laboratory, the preparation of the dry gel precursor is time-consuming and

energy-intensive, limiting its practical applications in industry. Moreover, the product quality is often nonuniform with the presence of low-crystalline impurities due to poor mass transfer.

3.3.3. Microwave- and Ultrasound-Assisted Methods

The choice of heating mode could also influence the morphology of SAPO-34. Compared with conventional oven heating, microwave irradiation might provide a rapid and uniform heat energy for the synthetic system, which effectively eliminates the undesired temperature gradient through dipole vibration of solvent and reactants. In this way, a higher concentration of nuclei and similar crystal growth rate may be reached, leading to small particles in uniform sizes. Up to now, TEAOH is the major choice of template for the studies on the microwave-assisted synthesis of SAPO-34, and the resultant crystal size was reported to be around 200 nm.[65] The crystallization time was shortened due to improved crystallization kinetics, and the Si incorporation level was also lowered leading to relatively mild acidity.[66] Additionally, Askari et al. succeeded in the preparation of SAPO-34 nanocrystals through sonochemical-assisted hydrothermal synthesis.[67] The generation of localized hot spots provided high temperature and pressure, which helped break the chemical bonds and accelerated the reaction.

3.3.4. Postsynthesis Treatment

Postsynthesis treatment is an effective top-down method to modulate the crystal properties. As an industrialized method,
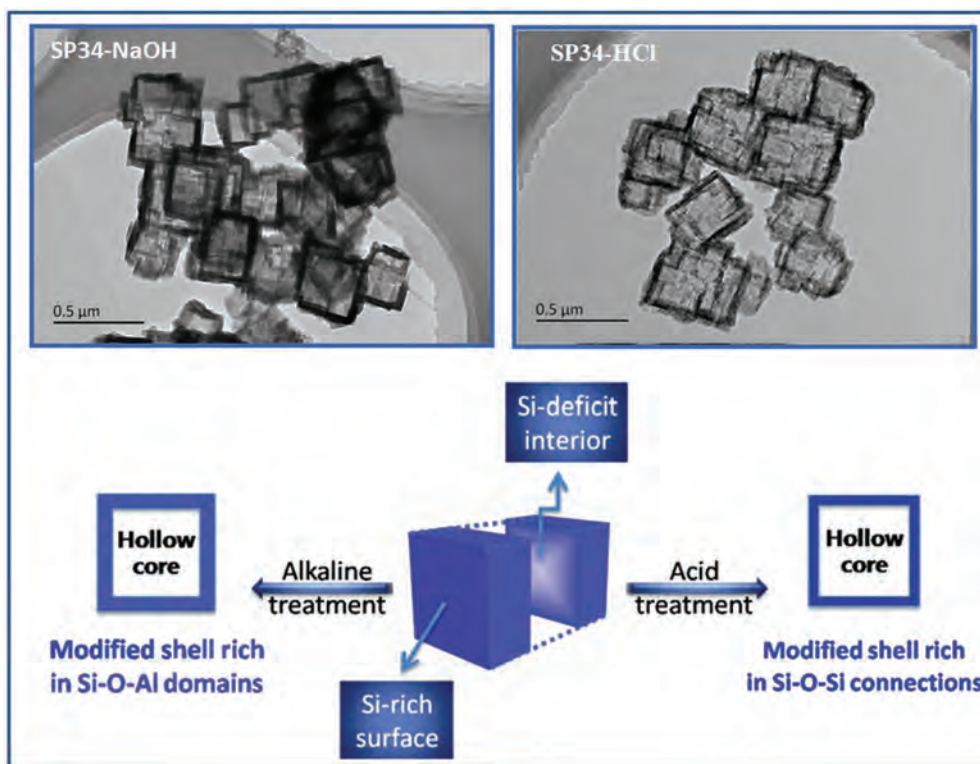
Figure 8. TEM images of hollow SAPO-34s achieved through the alkaline and acid treatments (up), and the proposed formation scheme (below). Reproduced with permission.[70] Copyright 2016, Royal Society of Chemistry.

dealumination by acid leaching or steaming treatment is often used to enhance the Si/Al ratios of aluminosilicate zeolites.[31a,b,68] Desilication in alkaline or fluoride media has been applied to introduce mesoporosity into zeolites. Unfortunately, all these strategies are difficult to be applied to the SAPO system because their framework structures are not as stable as those of aluminosilicates. To explore the opportunities of modifying SAPOs in this way, Verboekend et al. treated AlPO-5, SAPO-5, SAPO-11, and SAPO-34 by various acids and bases with the aim of creating mesopores.[69] The relative stability of zeotypes in basic media is rationalized through this work, which varies from very high for $H_{0.5}Si_{0.5}Al_{0.5}O_2$, to moderate SiO_2, to low $Al_{0.5}P_{0.5}O_2$. It demonstrates that the composition of parent molecular sieve is vital for its postprocessing results. Qiao et al. synthesized a special SAPO-34 parent with high Si content and abundant Si environments.[70] After a controlled acid or base etching, hollow SAPO-34 single crystals with a shell thickness of 30–50 nm and high crystallinity was successfully prepared. Si gradient in the parent crystals (increasing Si content from the core to the surface) was revealed to play an important role in the generation of hollow structure. The morphology of formed hollow SAPO-34 and the proposed formation mechanisms are shown in **Figure 8**. Chen et al. developed a fluoride route for the post treatment of SAPO-34 by using HF-NH_4F buffer solution.[71] They found that the treatment results were closely related with the choice of SAPO-34 parent. Hierarchical porous structures could be readily created in TEA-templated SAPO-34 due to a preferential dissolution of the Si-rich zones located on the highly defected interfaces

between crystalline domains. An improved MTO catalytic performance was observed for this sample. Liu et al. developed a facile TEAOH etching method to post treat SAPO-34 synthesized by TEA template.[72] After the treatment, the Si content decreased accompanied with a homogenous loss of Al and P; two kinds of pore patterns, i.e., scattered pores on the top and bottom surfaces and an hourglass-like pore pattern on the four side surfaces could be observed. Similar morphology was also achieved by an in situ growth etching method in TEA system developed by Xi et al.[73] These results demonstrated again the importance of parent SAPO-34 for postsynthesis treatment.

Although the improved MTO catalytic performance can be realized through a post-treatment strategy, solid yield and product crystallinity are usually sacrificed as expenses. Yang et al. developed a top-down strategy to prepare SAPO-34 nanocrystals with improved MTO catalytic property, as shown in **Figure 9**.[74] Conventional micrometer-sized SAPO-34 with a Si-enriched crystal surface was first milled to obtain a SAPO-34 precursor with low crystallinity and small particle size. The abundant structural subunits left in the precursor help them recrystallize quickly in an aluminophosphate solution or recycled mother liquid, leading to nanosized product in high solid yield and crystallinity. Moreover, the Si content of the recrystallized SAPO-34 was adjustable, and the surface Si enrichment was effectively attenuated due to the consumption of Si and the exposure of the interior of the precursor crystals. The reduced crystal size, decreased acid density, and attenuated surface Si enrichment resulted in a significantly prolonged lifetime together with an increased selectivity toward ethylene plus propylene.

**ADVANCED
SCIENCE NEWS**

www.advancedsciencenews.com

**ADVANCED
MATERIALS**

www.advmat.de
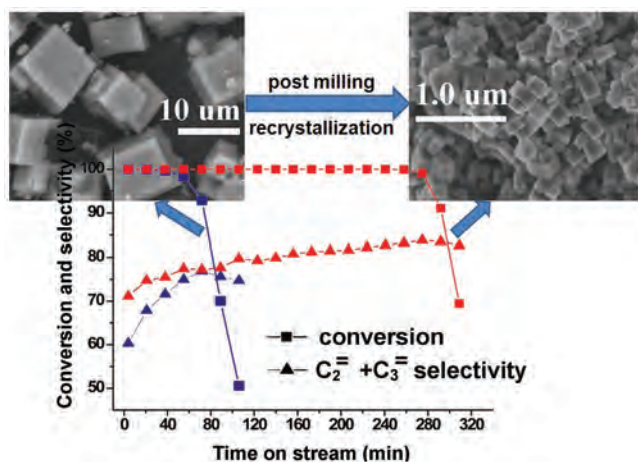
Figure 9. SEM images and MTO results of SAPO-34 before and after postsynthesis milling and recrystallization. Reaction conditions: T = 450 °C, WHSV = 4 h^{-1}, 40% methanol solution. Reproduced with permission.[74] Copyright 2014, Royal Society of Chemistry.

3.4. High Efficiency and Environment-Benign Synthesis of SAPO-34

Up to now, the industrial production of molecular sieves including SAPO-34 still adopts hydrothermal synthesis method. This process normally results in large amount of waste water and lower synthesis efficiency. Xi et al. reported a facile and green route for the synthesis of mesoporous SAPO-34 catalysts by recycling use of mother liquors.[75] After three recycles of mother liquors, the crystallinity, textural properties, acidity, as well as the excellent MTO catalytic performance of the mesoporous SAPO-34 were maintained well. However, the compositional variation of the mother liquid required a continuous input of composition analyses to compensate the insufficient nutrition. To improve the synthesis efficiency, Fan et al. developed an aminothermal synthesis approach, using organic amines as the main dispersing medium, as mentioned in Section 3.1.[41,42,76] Due to the presence of only stoichiometric amount of water, significantly improved solid yield was observed in this rather concentrated system. Moreover, the mother liquid, primarily comprising organic amines, could be easily recycled after distillation in the repeated synthesis batch. In addition, Jin et al. developed a solvent-free method to prepare SAPO-34, with advantages of low waste production and high solid yield.[77] Sun et al. used 20–50 nm SAPO-34 plates as seeds to synthesize SAPO-34.[78] The crystallization was believed to happen around the seeds which gradually dissolved and provided void space for crystal growth. The nanosized mesoporous SAPO-34 possessed a higher crystallinity, enhanced solid yield, and improved MTO catalytic performance. The discovery and use of effective seed-assisted method would provide more broad space for the synthesis optimization of SAPO-34.

An interesting attempt to fasten SAPO-34 synthesis is reported by Sun et al. recently.[79] With the aid of seeds, nanosized SAPO-34 was obtained in a stainless-steel tubular reactor with an inner diameter of 9.0 mm within 10 min. The remarkably reduced synthesis time was attributed to

the fast heat transfer of the stainless-steel tubular reactor in oil bath and rapid nucleation induced by the addition of SAPO-34 seeds. In addition, Okubo and co-workers reported the fast flow synthesis of SAPO-34 under the assistance of seeds.[80] With the development of new synthetic methods and the deepening mechanistic understanding of the crystallization process and MTO reaction, the synthesis efficiency of SAPO-34 with high catalytic performance is expected be continuously improved.

4. Toward Enhanced Ethylene or Propylene Selectivity

4.1. Enhancing the Propylene Selectivity

The prices of light olefins vary alternately with the fluctuating market demands, so it is highly desirable to steer the selectivity toward certain demanded olefin product, and the cost of product separation and purification will also be reduced. Hitherto, the reported propylene selectivity on molecular sieve catalysts is normally lower than 55%. In order to maximize the propylene production, Lurgi company developed a fixed bed MTP technology based on high-silica ZSM-5, in which alternative olefins other than propylene undergoes recirculation.[13] The accumulated propylene yield is around 65% (excluding H_2O). In addition, DICP developed a fluidized-bed DMTP technology for propylene production using SAPO-based catalyst by coupling three reaction processes including methanol conversion, alkylation of ethylene by methanol, and C_4^+ cracking processes. The pilot test (32 kg h^{-1} methanol) finished in 2015 gave a propylene selectivity of 75.0%, as well as 10.4% ethylene.[81] Tsinghua University developed the fluidized-bed FMTP technology in 2009 based on SAPO-18/34 catalyst, which integrated a methanol conversion unit and a coupling reaction unit for propylene and butylene, with a propylene selectivity of ≈67.3%.[82] Currently, both DMTP and FMTP technologies are yet to be commercialized.

Medium-pore ZSM-5 as the most popular catalyst for MTP reaction has received considerable attentions and investigations. The optimization strategies for ZSM-5-based MTP catalyst mainly focuses on two aspects: i) to decrease the acid density to promote the olefin-based cycle and consequently enhance the propylene selectivity; ii) to shorten the diffusion path by decreasing crystal size or introducing mesoporosity to prolong the catalyst lifetime. A variety of direct synthesis methods and postsynthesis treatments have been reported for the preparation of ZSM-5 catalyst to enhance its catalytic performance. Considering the ready existence of several relevant reviews, herein we will not further elaborate on it.[83]

Promoting olefin-based cycle to enhance propylene selectivity is also effective for large-pore zeolite catalyst. The research is mainly focused on high-silica Beta zeolite. Bjørgen et al. investigated the methanol conversion on dealuminated Beta (Si/Al = 120) at 350 °C.[19d] A high propylene/ethylene ratio of 21 was observed, but the propylene selectivity (22.7%) was relatively low. Both the aromatics and olefin cycles were revealed to function in the reaction.[19d,84] Otomo et al. prepared a series of dealuminated high-silica Beta via high-temperature calcination and acid treatment.[85] They found that the propylene selectivity

could achieve 37.4–49.7% over the material with a Si/Al ratio of 112. Very recently, Zhao et al. synthesized high-silica Beta zeolites with Si/Al ratio of 136–340, highlighted by their lower acid densities, under the assistance of HF.[27] Higher reaction temperature was found to favor the cracking of higher olefins and the propylene production, and the propylene selectivity could reach up to 58.3% at 550 °C. [12]C/^{13}C-methanol switch experiments revealed that the olefin methylation/cracking mechanism dominated the reaction. Afterward, hierarchical porous structure was further introduced into high-silica Beta by using a concentrated system.[86] The low water dosage was found to accelerate the nucleation and crystal growth rate, and promote the formation of nanoaggregates by preventing the further fusion of the primary grains. The hierarchical structure enhanced the accessibility of acid sites and molecular diffusion, leading to the reduced occurrence of side reactions and a prolonged MTP catalytic lifetime. In addition, CON-type boron-containing zeolite (Si/Al = 100–200) was also reported to exhibit ≈60% propylene selectivity as well as long catalyst lifetime.[87]

Compared to 10-MR and 12-MR zeolite catalysts, small pore SAPO molecular sieves with 8-MR windows have obvious superiority for ethylene and propylene production. However, the highest propylene selectivity reported for small-pore SAPO molecular sieves is below 50% together with low propylene/ethylene ratio (generally 0.8–2). This is because the aromatics cycle is dominant on the small pore molecular sieves such as SAPO-18 and SAPO-34 even with very low acid density. Very recently, the preliminary results from Yang et al. revealed that SAPO-14 molecular sieve with AFN topology and ultrasmall cage (5.3 × 10.5 Å) could catalyze the methanol conversion to achieve an unprecedented propylene selectivity of over 70% with a high propylene/ethylene ratio of 5–11.[88] The aromatics cycle in the ultrasmall AFN cage was greatly suppressed, and the olefin-based cycle was supposed to predominantly contribute to such a high propylene selectivity.

4.2. Enhancing the Ethylene Selectivity

Reports on promoting ethylene selectivity are relatively few. Previous mechanistic research demonstrates that ethylene is predominantly derived from methylbenzenes with two or three methyl groups, but propylene comes from those with four to six methyl groups.[20] It suggests the possibility to improve the ethylene selectivity through cavity modification, namely, controlling the active intermediates by the confinement effects of the host cavity. Recently, Zhang et al. reported that small pore zeolite H-RUB-50 with LEV cage exhibited higher selectivity for ethylene at 300 °C.[89] Based on theoretical calculations and experimental evidences, it was revealed that the steric confinement of LEV cage led to the formation of methylbenzenium and methylcyclopentenyl cations with fewer methyl groups, which acted as the active intermediates for the preferential production of ethylene. Generally, an ascending trend of the ethylene selectivity with time on stream could be observed for small pore molecular sieve catalysts, especially for SAPO-34 at higher reaction temperatures ($T \geq 450$ °C). It can be regarded as the result of the increased steric constraint by the incremental coke deposition. This implies the possibility of enhancing the

ethylene selectivity through precoking SAPO-34. Indeed, partially regenerated SAPO-34 with precisely controlled amount of hydrocarbon residuals has been adopted in the industrial DMTO process to improve the ethylene and ethylene plus propylene selectivity.[5] Moreover, Zhong et al. demonstrated that Zn cation-modified SAPO-34 catalysts prepared by ion exchange method have a promoting effect similar to the precoking approach.[90] The Zn cations accommodated in the cavities introduce extra diffusion limitation for hydrocarbons and increase the selectivity to ethylene and the ratio of ethylene to propylene in the MTO reaction. Until now, the highest ethylene selectivity achieved in the MTO reaction is normally below 60%. Previously, Inui and Kang reported a high ethylene selectivity as high as 88% on Ni-containing SAPO-34.[91] This interesting result, unfortunately, fails to be reproduced by the following researchers.

Very recently, Jiao et al. reported a highly selective preparation of ethylene from syngas using bifunctional oxide–zeolite (ZnCrO$_x$–mordenite) catalyst.[92] The reaction was revealed to proceed via ketene as an intermediate on the active sites of the mordenite 8-MR side pockets, leading to an ethylene selectivity (excluding CO$_2$) up to 73% at a CO conversion of 26%. Given that acetyl group (a physically adsorbed protonated ketene on Brønsted acid sites) has been confirmed to link the direct and aromatic mechanisms in the MTO reaction,[93] it is supposed that the reaction intermediates over zeolite in the STO process may be comparable to that of the MTO process. These results suggest the possibility of regulating the MTO product selectivity by altering the reaction conditions (e.g., cofeeding with other gases or coupling other functional components). Moreover, a prolonged MTO catalytic lifetime was reported recently for the physical mixtures of metal oxide with SAPO-34 catalyst, for example MgO[94] and Y$_2$O$_3$[95] with SAPO-34. The metal oxide catalyzes the dehydrogenation of methanol to formaldehyde which transports between and within zeotypic/zeolitic domains affecting the reaction pathway and catalyst lifetime.

5. Conclusions and Outlook

The large-scale industrialization of the MTO process in the last decade has triggered a new round of worldwide research interests in the MTO reaction mechanism and molecular sieve catalyst. Intensive investigations together with the development of in situ characterization techniques greatly deepen the fundamental understanding of the reaction mechanism, including the formation of initial C−C bond. The progress on the MTO reaction mechanism not only facilitates the technology development, but also offers useful guidelines for the catalyst design and optimization. Meanwhile, important advances are achieved in the rational synthesis of molecular sieves with controlled acidity and pore architectures, which significantly contributes to the further optimization of MTO catalyst.

The topologies and acid properties of molecular sieve catalysts are the key factors influencing their MTO catalytic performance, which determine the reaction routes and product selectivity. Up to now, SAPO-34 is still the most effective catalyst for the MTO reaction. Although SAPO-34-based catalyst is already extensively employed in the commercial MTO process, it is highly desirable to further improve its catalytic performance and

synthesis efficiency. The future research might include: 1) to synthesize nanosized or mesoporous SAPO-34 with high quality, in which the Si content, Si distribution, pore connectivity, and hydrothermal stability should be well-controlled simultaneously; 2) to develop effective fluoride-free strategies to synthesize low-silica SAPO-34 with high crystallinity and tunable Si content, and elucidate the acidity-performance correlation for catalysts of low acid density; 3) to couple other functional components with SAPO-34 to optimize the reaction pathway and improve the catalytic performance; 4) to develop cost-efficient and environment-friendly synthesis methods feasible for industrial scale-up production. In addition, to meet the fluctuating market demand for ethylene or propylene, it is valuable to develop specialized catalysts with preferential ethylene or propylene yield. Progress in this aspect is currently limited, which mainly depends on the recycling reaction of undesired olefin products. The application of new materials with appropriate topology (cavity size and pore opening) and low acid density might provide more opportunities to maximize the yield for a specific product.

The breakthrough in syngas to olefins in recent years brings new inspirations for the MTO process and its catalyst design. The composite catalyst (oxides and zeolites) can effectively transform syngas to light olefins ($C_2^=$—$C_4^=$, ≈80% selectivity excluding CO_2) with high ethylene selectivity (≈73% selectivity)[92] or with long catalyst lifetime (>100 h).[96] The extended catalyst lifetime is likely related with the hydrogenation ability of acid sites on zeolites under high H_2 pressure.[97] These works also imply the possibility of prolonging the MTO reaction lifetime or tuning the product selectivity by changing the reaction conditions.

Acknowledgements

Conflict of Interest

The authors declare no conflict of interest.

Keywords

[1] a) J. Čejka, A. Corma, F. Schüth, *Introduction to Zeolite Science and Practice*, Elsevier B.V., Amsterdam, The Netherlands **2007**; b) A. Corma, *J. Catal.* **2003**, *216*, 298.

[2] C. D. Chang, W. H. Lang, *US4025576 A*, **1977**.

[3] a) U. Olsbye, S. Svelle, M. Bjorgen, P. Beato, T. V. W. Janssens, F. Joensen, S. Bordiga, K. P. Lillerud, *Angew. Chem., Int. Ed.* **2012**,
51, 5810; b) D. Chen, K. Moljord, A. Holmen, *Microporous Mesoporous Mater.* **2012**, *164*, 239; c) S. Xu, Y. Zhi, J. Han, W. Zhang, X. Wu, T. Sun, Y. Wei, Z. Liu, in *Advances in Catalysis*, Vol. *61*, (Ed: C. Song), Academic Press, Burlington, MA, USA **2017**, p. 37; d) I. Yarulina, A. D. Chowdhury, F. Meirer, B. M. Weckhuysen, J. Gascon, *Nat. Catal.* **2018**, *1*, 398.

[4] a) J. Zhong, J. Han, Y. Wei, P. Tian, X. Guo, C. Song, Z. Liu, *Catal. Sci. Technol.* **2017**, *7*, 4905; b) Q. Sun, Z. Xie, J. Yu, *Natl. Sci. Rev.* **2018**, *5*, 542.

[5] P. Tian, Y. Wei, M. Ye, Z. Liu, *ACS Catal.* **2015**, *5*, 1922.

[6] a) M. Moliner, C. Martinez, A. Corma, *Chem. Mater.* **2014**, *26*, 246; b) M. Dusselier, M. E. Davis, *Chem. Rev.* **2018**, *118*, 5265.

[7] Z. Liu, J. Liang, *Curr. Opin. Solid State Mater. Sci.* **1999**, *4*, 80.

[8] J. Liang, H. Y. Li, S. Zhao, W. G. Guo, R. H. Wang, M. L. Ying, *Appl. Catal.* **1990**, *64*, 31.

[9] a) A. J. Marchi, G. F. Froment, *Appl. Catal.* **1991**, *71*, 139; b) M. Briend, R. Vomscheid, M. J. Peltre, P. P. Man, D. Barthomeuf, *J. Phys. Chem.* **1995**, *99*, 8270.

[10] A. M. Rouhi, *C&EN* **2015**, *93*, 30.

[11] B. V. Vora, T. L. Marker, P. T. Barger, H. R. Nilsen, S. Kvisle, T. Fuglerud, in *Surface Science and Catalysis*, Vol. *107* (Eds: M. dePontes, R. L. Espinoza, C. P. Nicolaides, J. H. Scholtz, M. S. Scurrell), Elsevier, Amsterdam, The Netherlands **1997**, p. 87.

[12] Q. Chen, W. Yang, J. Teng, *Chin. J. Catal.* **2013**, *34*, 217.

[13] H. Koempel, W. Liebner, in *Proc. of the 8th Natural Gas Conversion Symp.*, Vol. *167* (Eds: F. B. Noronha, M. Schmal, E. F. Sousa-Aguiar), Elsevier, Amsterdam, The Netherlands **2007**, p. 261.

[14] a) X. Wu, S. Xu, W. Zhang, J. Huang, J. Li, B. Yu, Y. Wei, Z. Liu, *Angew. Chem., Int. Ed.* **2017**, *56*, 9039; b) X. Wu, S. Xu, Y. Wei, W. Zhang, J. Huang, S. Xu, Y. He, S. Lin, T. Sun, Z. Liu, *ACS Catal.* **2018**, *8*, 7356.

[15] Y. Liu, S. Mueller, D. Berger, J. Jelic, K. Reuter, M. Tonigold, M. Sanchez-Sanchez, J. A. Lercher, *Angew. Chem., Int. Ed.* **2017**, *56*, 7342.

[16] J. Li, Z. Wei, Y. Chen, B. Jing, Y. He, M. Dong, H. Jiao, X. Li, Z. Qin, J. Wang, W. Fan, *J. Catal.* **2014**, *317*, 277.

[17] N. Tajima, T. Tsuneda, F. Toyama, K. Hirao, *J. Am. Chem. Soc.* **1998**, *120*, 8222.

[18] A. D. Chowdhury, K. Houben, G. T. Whiting, M. Mokhtar, A. M. Asiri, S. A. Al-Thabaiti, S. N. Basahel, M. Baldus, B. M. Weckhuysen, *Angew. Chem., Int. Ed.* **2016**, *55*, 15840.

[19] a) S. Svelle, F. Joensen, J. Nerlov, U. Olsbye, K.-P. Lillerud, S. Kolboe, M. Bjorgen, *J. Am. Chem. Soc.* **2006**, *128*, 14770; b) M. Bjorgen, S. Svelle, F. Joensen, J. Nerlov, S. Kolboe, F. Bonino, L. Palumbo, S. Bordiga, U. Olsbye, *J. Catal.* **2007**, *249*, 195; c) D. Lesthaeghe, A. Horre, M. Waroquier, G. B. Marin, V. Van Speybroeck, *Chem. - Eur. J.* **2009**, *15*, 10803; d) M. Bjørgen, F. Joensen, K.-P. Lillerud, U. Olsbye, S. Svelle, *Catal. Today* **2009**, *142*, 90.

[20] a) W. Song, H. Fu, J. F. Haw, *J. Am. Chem. Soc.* **2001**, *123*, 4749; b) C. Wang, J. Xu, G. Qi, Y. Gong, W. Wang, P. Gao, Q. Wang, N. Feng, X. Liu, F. Deng, *J. Catal.* **2015**, *332*, 127.

[21] a) J. Li, Y. Wei, J. Chen, P. Tian, X. Su, S. Xu, Y. Qi, Q. Wang, Y. Zhou, Y. He, Z. Liu, *J. Am. Chem. Soc.* **2012**, *134*, 836; b) J. Chen, J. Li, Y. Wei, C. Yuan, B. Li, S. Xu, Y. Zhou, J. Wang, M. Zhang, Z. Liu, *Catal. Commun.* **2014**, *46*, 36; c) J. Li, Y. Wei, J. Chen, S. Xu, P. Tian, X. Yang, B. Li, J. Wang, Z. Liu, *ACS Catal.* **2015**, *5*, 661.

[22] I. Pinilla-Herrero, U. Olsbye, C. Marquez-Alvarez, E. Sastre, *J. Catal.* **2017**, *352*, 191.

[23] S. Hu, J. Shan, Q. Zhang, Y. Wang, Y. Liu, Y. Gong, Z. Wu, T. Dou, *Appl. Catal., A* **2012**, *445–446*, 215.

[24] J. Wang, J. Li, S. Xu, Y. Zhi, Y. Wei, Y. He, J. Chen, M. Zhang, Q. Wang, W. Zhang, X. Wu, X. Guo, Z. Liu, *Chin. J. Catal.* **2015**, *36*, 1392.

[25] A. Sassi, M. A. Wildman, H. J. Ahn, P. Prasad, J. B. Nicholas, J. F. Haw, *J. Phys. Chem. B* **2002**, *106*, 2294.

ADVANCED
SCIENCE NEWS
www.advancedsciencenews.com

ADVANCED
MATERIALS
www.advmat.de

[26] Z. Liu, X. Dong, Y. Zhu, A. Emwas, D. Zhang, Q. Tian, Y. Han, *ACS Catal.* **2015**, *5*, 5837.

[27] X. Zhao, L. Wang, J. Li, S. Xu, W. Zhang, Y. Wei, X. Guo, P. Tian, Z. Liu, *Catal. Sci. Technol.* **2017**, *7*, 5882.

[28] a) M. Guisnet, L. Costa, F. R. Ribeiro, *J. Mol. Catal. A: Chem.* **2009**, *305*, 69; b) D. Mores, J. Kornatowski, U. Olsbye, B. M. Weckhuysen, *Chem. - Eur. J.* **2011**, *17*, 2874; c) I. Yarulina, S. Bailleul, A. Pustovarenko, J. R. Martinez, K. De Wispelaere, J. Hajek, B. M. Weckhuysen, K. Houben, M. Baldus, V. Van Speybroeck, F. Kapteijn, J. Gascon, *ChemCatChem* **2016**, *8*, 3057.

[29] J. Chen, J. Li, C. Yuan, S. Xu, Y. Wei, Q. Wang, Y. Zhou, J. Wang, M. Zhang, Y. He, S. Xu, Z. Liu, *Catal. Sci. Technol.* **2014**, *4*, 3268.

[30] B. Gao, M. Yang, Y. Qiao, J. Li, X. Xiang, P. Wu, Y. Wei, S. Xu, P. Tian, Z. Liu, *Catal. Sci. Technol.* **2016**, *6*, 7569.

[31] a) S. Lopez-Orozco, A. Inayat, A. Schwab, T. Selvam, W. Schwieger, *Adv. Mater.* **2011**, *23*, 2602; b) V. Valtchev, G. Majano, S. Mintova, J. Perez-Ramirez, *Chem. Soc. Rev.* **2013**, *42*, 263; c) V. Valtchev, L. Tosheva, *Chem. Rev.* **2013**, *113*, 6734.

[32] a) D. Chen, K. Moljord, T. Fuglerud, A. Holmen, *Microporous Mesoporous Mater.* **1999**, *29*, 191; b) G. Yang, Y. Wei, S. Xu, J. Chen, J. Li, Z. Li, J. Yu, R. Xu, *J. Phys. Chem. C* **2013**, *117*, 8214.

[33] M. Bjorgen, F. Joensen, M. S. Holm, U. Olsbye, K.-P. Lillerud, S. Svelle, *Appl. Catal., A* **2008**, *345*, 43.

[34] a) K. Barbera, F. Bonino, S. Bordiga, T. V. W. Janssens, P. Beato, *J. Catal.* **2011**, *280*, 196; b) I. Yarulina, J. Goetze, C. Gucuyener, L. van Thiel, A. Dikhtiarenko, J. Ruiz-Martinez, B. M. Weckhuysen, J. Gascon, F. Kapteijn, *Catal. Sci. Technol.* **2016**, *6*, 2663; c) X. Meng, M. Zhang, C. Chen, C. Li, W. Xiong, M. Li, *Appl. Catal., A* **2018**, *558*, 122.

[35] D. Barthomeuf, *Zeolites* **1994**, *14*, 394.

[36] R. Vomscheid, M. Briend, M. J. Peltre, P. P. Man, D. Barthomeuf, *J. Phys. Chem.* **1994**, *98*, 9614.

[37] a) Y. Wang, S. Chen, Y.-J. Jiang, Y. Cao, F. Chen, W.-K. Chang, Y.-L. Gao, *RSC Adv.* **2016**, *6*, 104985; b) R. L. Smith, W. A. Slawinski, A. Lind, D. S. Wragg, J. H. Cavka, B. Arstad, H. Fjellvag, M. P. Attfield, D. Akporiaye, M. W. Anderson, *Chem. Mater.* **2015**, *27*, 4205.

[38] M. Janssen, A. Verberckmoes, M. Mertens, A. Bons, W. Mortier, EP1365992 B1, **2007**.

[39] P. Wu, M. Yang, W. Zhang, S. Xu, P. Guo, P. Tian, Z. Liu, *Chem. Commun.* **2017**, *53*, 4985.

[40] a) G. Liu, P. Tian, J. Li, D. Zhang, F. Zhou, Z. Liu, *Microporous Mesoporous Mater.* **2008**, *111*, 143; b) A. M. Prakash, S. Unnikrishnan, *J. Chem. Soc., Faraday Trans.* **1994**, *90*, 2291.

[41] D. Fan, P. Tian, S. Xu, Q. Xia, X. Su, L. Zhang, Y. Zhang, Y. He, Z. Liu, *J. Mater. Chem.* **2012**, *22*, 6568.

[42] a) D. Fan, P. Tian, X. Su, Y. Yuan, D. Wang, C. Wang, M. Yang, L. Wang, S. Xu, Z. Liu, *J. Mater. Chem. A* **2013**, *1*, 14206; b) D. Wang, P. Tian, M. Yang, S. Xu, D. Fan, X. Su, Y. Yang, C. Wang, Z. Liu, *Microporous Mesoporous Mater.* **2014**, *194*, 8.

[43] D. Fan, P. Tian, S. Xu, D. Wang, Y. Yang, J. Li, Q. Wang, M. Yang, Z. Liu, *New J. Chem.* **2016**, *40*, 4236.

[44] N. Yan, H. Xu, W. Zhang, T. Sun, P. Guo, P. Tian, Z. Liu, *Microporous Mesoporous Mater.* **2018**, *264*, 55.

[45] N. Yan, L. Wang, X. Liu, P. Wu, T. Sun, S. Xu, J. Han, P. Guo, P. Tian, Z. Liu, *J. Mater. Chem. A* **2018**, *6*, 24186.

[46] E. Maria Gallego, M. Teresa Portilla, C. Paris, A. Leon-Escamilla, M. Boronat, M. Moliner, A. Corma, *Science* **2017**, *355*, 1051.

[47] C. Li, C. Paris, J. Martinez-Triguero, M. Boronat, M. Moliner, A. Corma, *Nat. Catal.* **2018**, *1*, 547.

[48] a) S. Oliver, A. Kuperman, G. A. Ozin, *Angew. Chem., Int. Ed.* **1998**, *37*, 46; b) J. Wu, H. Zhao, N. Li, Q. Luo, C. He, N. Guan, S. Xiang, *CrystEngComm* **2012**, *14*, 8671.

[49] W. Dai, G. Cao, L. Yang, G. Wu, M. Dyballa, M. Hunger, N. Guan, L. Li, *Catal. Sci. Technol.* **2017**, *7*, 607.

[50] L. Xu, A. Du, Y. Wei, S. Meng, Y. He, Y. Wang, Z. Yu, X. Zhang, Z. Liu, *Chin. J. Catal.* **2008**, *29*, 727.

[51] B. Gao, P. Tian, M. Li, M. Yang, Y. Qiao, L. Wang, S. Xu, Z. Liu, *J. Mater. Chem. A* **2015**, *3*, 7741.

[52] a) Q. Sun, N. Wang, D. Xi, M. Yang, J. Yu, *Chem. Commun.* **2014**, *50*, 6502; b) C. Wang, M. Yang, P. Tian, S. Xu, Y. Yang, D. Wang, Y. Yuan, Z. Liu, *J. Mater. Chem. A* **2015**, *3*, 5608; c) C. Wang, *Ph.D. Thesis, Dalian Institute of Chemical Physics, CAS* **2016**; d) H. Chen, M. Wang, M. Yang, W. Shang, C. Yang, B. Liu, Q. Hao, J. Zhang, X. Ma, *J. Mater. Sci.* **2019**, *54*, 8202.

[53] C. Wang, M. Yang, M. Li, S. Xu, Y. Yang, P. Tian, Z. Liu, *Chem. Commun.* **2016**, *52*, 6463.

[54] B. Yang, P. Zhao, J. Ma, R. Li, *Chem. Phys. Lett.* **2016**, *665*, 59.

[55] J. Zheng, J. Ding, D. Jin, G. Ye, K. Zhu, X. Zhou, W. Yang, W. Yuan, *Chem. Commun.* **2017**, *53*, 6132.

[56] C. Wang, M. Yang, W. Zhang, X. Su, S. Xu, P. Tian, Z. Liu, *RSC Adv.* **2016**, *6*, 47864.

[57] P. Wu, M. Yang, L. Sun, S. Zeng, S. Xu, P. Tian, Z. Liu, *Chem. Commun.* **2018**, *54*, 11160.

[58] G. Guo, Q. Sun, N. Wang, R. Bai, J. Yu, *Chem. Commun.* **2018**, *54*, 3697.

[59] J. Gong, C. Wang, C. Zeng, L. Zhang, *Microporous Mesoporous Mater.* **2016**, *221*, 128.

[60] S. Lin, J. Li, R. P. Sharma, J. Yu, R. Xu, *Top. Catal.* **2010**, *53*, 1304.

[61] J. Zhu, Y. Cui, Y. Wang, F. Wei, *Chem. Commun.* **2009**, 3282.

[62] Y. Hirota, K. Murata, S. Tanaka, N. Nishiyama, Y. Egashira, K. Ueyama, *Mater. Chem. Phys.* **2010**, *123*, 507.

[63] S. Rimaz, R. Halladj, S. Askari, *J. Colloid Interface Sci.* **2016**, *464*, 137.

[64] J. Gong, F. Tong, X. Ji, C. Zeng, C. Wang, Y. Lv, L. Zhang, *Cryst. Growth Des.* **2014**, *14*, 3857.

[65] a) H. van Heyden, S. Mintova, T. Bein, *Chem. Mater.* **2008**, *20*, 2956; b) T. Alvaro-Munoz, E. Sastre, C. Marquez-Alvarez, *Catal. Sci. Technol.* **2014**, *4*, 4330.

[66] S.-T. Yang, J.-Y. Kim, H.-J. Chae, M. Kim, S.-Y. Jeong, W.-S. Ahn, *Mater. Res. Bull.* **2012**, *47*, 3888.

[67] a) S. Askari, S. M. Alipour, R. Halladj, M. H. D. A. Farahani, *J. Porous Mater.* **2013**, *20*, 285; b) S. Askari, R. Halladj, *J. Solid State Chem.* **2013**, *201*, 85; c) S. Askari, R. Halladj, M. Nazari, *Mater. Res. Bull.* **2013**, *48*, 1851.

[68] W. Schwieger, A. G. Machoke, T. Weissenberger, A. Inayat, T. Selvam, M. Klumpp, A. Inayat, *Chem. Soc. Rev.* **2016**, *45*, 3353.

[69] D. Verboekend, M. Milina, J. Perez-Ramirez, *Chem. Mater.* **2014**, *26*, 4552.

[70] Y. Qiao, M. Yang, B. Gao, L. Wang, P. Tian, S. Xu, Z. Liu, *Chem. Commun.* **2016**, *52*, 5718.

[71] X. Chen, A. Vicente, Z. Qin, V. Ruaux, J.-P. Gilson, V. Valtchev, *Chem. Commun.* **2016**, *52*, 3512.

[72] X. Liu, S. Ren, G. Zeng, G. Liu, P. Wu, G. Wang, X. Chen, Z. Liu, Y. Sun, *RSC Adv.* **2016**, *6*, 28787.

[73] D. Xi, Q. Sun, J. Xu, M. Cho, H. S. Cho, S. Asahina, Y. Li, F. Deng, O. Terasaki, J. Yu, *J. Mater. Chem. A* **2014**, *2*, 17994.

[74] M. Yang, P. Tian, C. Wang, Y. Yuan, Y. Yang, S. Xu, Y. He, Z. Liu, *Chem. Commun.* **2014**, *50*, 1845.

[75] D. Xi, Q. Sun, X. Chen, N. Wang, J. Yu, *Chem. Commun.* **2015**, *51*, 11987.

[76] B. Gao, D. Fan, L. Sun, H. An, F. Fan, S. Xu, P. Tian, Z. Liu, *Microporous Mesoporous Mater.* **2017**, *248*, 204.

[77] Y. Jin, Q. Sun, G. Qi, C. Yang, J. Xu, F. Chen, X. Meng, F. Deng, F. Xiao, *Angew. Chem., Int. Ed.* **2013**, *52*, 9172.

[78] a) Q. Sun, N. Wang, R. Bai, X. Chen, J. Yu, *J. Mater. Chem. A* **2016**, *4*, 14978; b) Q. Sun, N. Wang, R. Bai, G. Chen, Z. Shi, Y. Zou, J. Yu, *ChemSusChem* **2018**, *11*, 3812.

[79] Q. Sun, N. Wang, G. Guo, J. Yu, *Chem. Commun.* **2015**, *51*, 16397.

[80] Z. Liu, T. Wakihara, N. Nomura, T. Matsuo, C. Anand, S. P. Elangovan, Y. Yanaba, T. Yoshikawa, T. Okubo, *Chem. Mater.* **2016**, *28*, 4840.

**ADVANCED
SCIENCE NEWS**

www.advancedsciencenews.com

**ADVANCED
MATERIALS**

www.advmat.de

[81] Methanol to propylene new technology (DMTP), http://www.dicp.cas.cn/kycg_1/yyyjcg/201811/t20181129_5201102.html (accessed: August 2018).

[82] a) J. Zhu, Y. Cui, Y. Chen, H. Zhou, Y. Wang, F. Wei, *J. Chem. Ind. Eng.* **2010**, *61*, 1674; b) Y. Wang, F. Wei, Z. Qian, X. Yuan, H. Zhou, J. Liu, *China 1962573 A*, **2006**.

[83] a) A. Galadima, O. Muraza, *Ind. Eng. Chem. Res.* **2015**, *54*, 4891; b) H. Pan, M. Tian, Z. He, K. Hua, Q. Lin, *Chem. Ind. Eng. Prog.* **2014**, *33*, 2625; c) T. Sano, *J. Jpn. Pet. Inst.* **2017**, *60*, 263.

[84] J. Zhang, Z. Huang, P. Li, X. Zhang, X. Zhang, Y. Yuan, L. Xu, *Catal. Sci. Technol.* **2017**, *7*, 2194.

[85] R. Otomo, U. Mueller, M. Feyen, B. Yilmaz, X. Meng, F.-S. Xiao, H. Gies, X. Bao, W. Zhang, D. De Vosh, T. Yokoi, *Catal. Sci. Technol.* **2016**, *6*, 713.

[86] X. Zhao, L. Wang, P. Guo, N. Yan, T. Sun, S. Lin, X. Guo, P. Tian, Z. Liu, *Catal. Sci. Technol.* **2018**, *8*, 2966.

[87] M. Yoshioka, T. Yokoi, T. Tatsumi, *ACS Catal.* **2015**, *5*, 4268.

[88] a) M. Yang, P. Tian, Z. Liu, B. Li, L. Liu, S. Sang, *China 201711232744.6*, **2017**; b) M. Yang, B. Li, S. Lin, M. Gao, X. Zhao, S. Xu, Y. Wei, P. Guo, P. Tian, Z. Liu, presented at *19th Int. Zeolite Conf.*, Perth, Australia, July **2019**.

[89] W. Zhang, J. Chen, S. Xu, Y. Chu, Y. Wei, Y. Zhi, J. Huang, A. Zheng, X. Wu, X. Meng, F. Xiao, F. Deng, Z. Liu, *ACS Catal.* **2018**, *8*, 10950.

[90] J. Zhong, J. Han, Y. Wei, S. Xu, Y. He, Y. Zheng, M. Ye, X. Guo, C. Song, Z. Liu, *Chem. Commun.* **2018**, *54*, 3146.

[91] T. Inui, M. Kang, *Appl. Catal., A* **1997**, *164*, 211.

[92] F. Jiao, X. Pan, K. Gong, Y. Chen, G. Li, X. Bao, *Angew. Chem., Int. Ed.* **2018**, *57*, 4692.

[93] a) A. D. Chowdhury, A. L. Paioni, K. Houben, G. T. Whiting, M. Baldus, B. M. Weckhuysen, *Angew. Chem., Int. Ed.* **2018**, *57*, 8095; b) A. D. Chowdhury, J. Gascon, *Angew. Chem., Int. Ed.* **2018**, *57*, 14982.

[94] Y. Wang, S. Chen, Y. Gao, Y. Cao, Q. Zhang, W. Chang, J. Benziger, *ACS Catal.* **2017**, *7*, 5572.

[95] A. Hwang, A. Bhan, *ACS Catal.* **2017**, *7*, 4417.

[96] a) F. Jiao, J. Li, X. Pan, J. Xiao, H. Li, H. Ma, M. Wei, Y. Pan, Z. Zhou, M. Li, S. Miao, J. Li, Y. Zhu, D. Xiao, T. He, J. Yang, F. Qi, Q. Fu, X. Bao, *Science* **2016**, *351*, 1065; b) K. Cheng, B. Gu, X. Liu, J. Kang, Q. Zhang, Y. Wang, *Angew. Chem., Int. Ed.* **2016**, *55*, 4725.

[97] a) S. S. Arora, D. L. S. N. Ieskens, A. Malek, A. Bhan, *Nat. Catal.* **2018**, *1*, 666; b) X. Zhao, J. Li, P. Tian, L. Wang, X. Li, S. Lin, X. Guo, Z. Liu, *ACS Catal.* **2019**, *9*, 3017.